Reversible Hydrogen Storage by $NaAlH_4$ Confined within a Titanium-Functionalized MOF-74(Mg) Nanoreactor

Vitalie Stavila,[†,*] Raghunandan K. Bhakta,[†] Todd M. Alam,[‡] Eric H. Majzoub,[§] and Mark D. Allendorf[†,*]

[†]Sandia National Laboratories, Livermore, California 94551-0969, United States, [‡]Sandia National Laboratories, Albuquerque, New Mexico 87185, United States, and [§]Center for Nanoscience, and Department of Physics and Astronomy, University of Missouri, St. Louis, Missouri 63130, United States

ABSTRACT We demonstrate that $NaAlH_4$ confined within the nanopores of a titanium-functionalized metal–organic framework (MOF) template MOF-74(Mg) can reversibly store hydrogen with minimal loss of capacity. Hydride-infiltrated samples were synthesized by melt infiltration, achieving loadings up to 21 wt %. MOF-74(Mg) possesses one-dimensional, 12 Å channels lined with Mg atoms having open coordination sites, which can serve as sites for Ti catalyst stabilization. MOF-74(Mg) is stable under repeated hydrogen desorption and hydride regeneration cycles, allowing it to serve as a "nanoreactor". Confining $NaAlH_4$ within these pores alters the decomposition pathway by eliminating the stable intermediate Na_3AlH_6 phase observed during bulk decomposition and proceeding directly to NaH, Al, and H_2, in agreement with theory. The onset of hydrogen desorption for both Ti-doped and undoped nano-$NaAlH_4$@MOF-74(Mg) is ~50 °C, nearly 100 °C lower than bulk $NaAlH_4$. However, the presence of titanium is not necessary for this increase in desorption kinetics but enables rehydriding to be almost fully reversible. Isothermal kinetic studies indicate that the activation energy for H_2 desorption is reduced from 79.5 kJ mol^{-1} in bulk Ti-doped $NaAlH_4$ to 57.4 kJ mol^{-1} for nanoconfined $NaAlH_4$. The structural properties of nano-$NaAlH_4$@MOF-74(Mg) were probed using ^{23}Na and ^{27}Al solid-state MAS NMR, which indicates that the hydride is not decomposed during infiltration and that Al is present as tetrahedral AlH_4^- anions prior to desorption and as Al metal after desorption. Because of the highly ordered MOF structure and monodisperse pore dimensions, our results allow key template features to be identified to ensure reversible, low-temperature hydrogen storage.

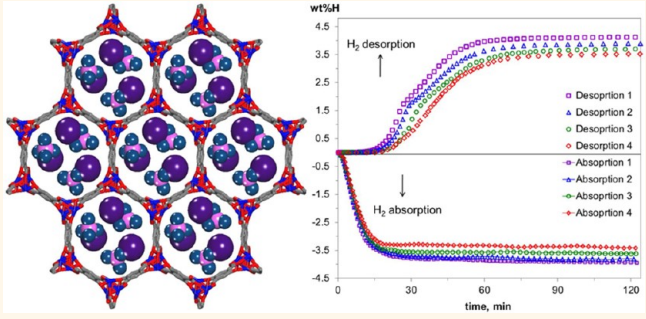

KEYWORDS: metal–organic frameworks · nanoreactors · metal hydrides · hydrogen storage · reversibility · nanoconfinement

It is now well-established that confining metal hydrides within a nanoporous material accelerates their hydrogen desorption kinetics[1−6] and in some cases alters the thermodynamics[5,7−9] of the process as well. However, the question of whether such hybrid storage materials can be of practical use is still outstanding. Aside from the fact that the template reduces the gravimetric capacity of the storage material (although it may increase its volumetric capacity if a sufficiently low-density scaffold is used), there is only limited evidence that nanoscale hydrides can be used reversibly.[1,4−6,10−12] Bulk complex metal hydrides typically require high H_2 pressures to drive the rehydrogenation reaction, which makes on-board regeneration unfeasible. The concept of reversible hydrogen storage in complex metal hydrides was first demonstrated by Bogdanovic and Schwickardi[13] using Ti-doped $NaAlH_4$, and this has become a canonical system for solid-state H_2 storage. The decomposition of bulk $NaAlH_4$ takes place in two steps and includes the formation of a stable intermediate, Na_3AlH_6:

$$NaAlH_4 \underset{\text{step1}}{\overset{[Cat.]}{\rightleftharpoons}} 1/3Na_3AlH_6 + 2/3Al + H_2 \underset{\text{step2}}{\overset{[Cat.]}{\rightleftharpoons}} NaH + Al + 1/2H_2 \quad (1)$$

Addition of a catalyst (Ti or other transition metal) is necessary for both steps 1 and 2 to be reversible under practical conditions. In contrast, nanoconfined $NaAlH_4$ decomposes in a single step without the need for a catalyst,

* Address correspondence to vnstavi@sandia.gov, mdallen@sandia.gov.

Received for review July 25, 2012 and accepted October 17, 2012.

Published online October 17, 2012
10.1021/nn304514c

as shown by both density functional theory (DFT) calculations[14,15] and several experimental reports.[5−7,12]

Reports concerning reversibility of nanoconfined hydrides are much more sparse, however. Nielsen *et al.* demonstrated that $NaAlH_4$ within nanoporous carbon aerogel (average pore size 17 nm) can be partially regenerated by incorporating $TiCl_3$ catalyst within the pores. However, the reversible capacity drops precipitously to about 50% within four cycles.[1] Xiong *et al.* found that $NaAlH_4$ infiltrated into $Ti(OBu)_4$-loaded ordered mesoporous carbon retains approximately 80% of the initial H_2 capacity after 11 dehydrogenation/rehydrogenation cycles.[16] In another report, Zheng *et al.* regenerated ~67% of the original hydrogen capacity by rehydrogenating $NaAlH_4$ in mesoporous silica (average pore size 10 nm) without a catalyst at 150 °C and 5.5 MPa H_2 pressure,[17] conditions under which $NaAlH_4$ is not reversible. Finally, Gao and co-workers studied the hydrogen desorption from $NaAlH_4$ confined in 2−3 nm pores of carbon and reported improved kinetics but also partial reversibility as low as 2.4 MPa H_2 and 160 °C.[5]

While these studies demonstrate that nanoconfinement can increase the kinetics of hydride regeneration under moderate conditions, the partial reversibility and/or significant capacity losses observed indicate that a much better understanding of the factors influencing reversibility at the nanoscale is required to develop effective nanoscale hydride storage materials. It should also be mentioned that Pinkerton *et al.* melt-infiltrated $NaAlH_4$ into 13-nm carbon aerogels and observed enhanced H_2 release kinetics and up to 85% reversibility at 10.0 MPa H_2 and 160 °C.[18] However, in this case, it is clear that the observed effects are not solely due to confinement, as the enhanced behavior was observed in samples having too small a pore volume to accommodate all of the hydride in the sample. In addition, the reaction apparently occurs by the normal two-step decomposition process shown above in reaction 1, compared with the one-step decomposition seen for nanoconfined $NaAlH_4$.

In our own work, we recently demonstrated that infiltrating $NaAlH_4$ into the pores of the metal−organic framework (MOF) $Cu_3(btc)_2$ (btc = 1,3,5-benzenetricarboxylate) results in remarkable changes in both kinetics and thermodynamics of hydrogen release.[2,7] MOFs are attractive as supports for hydride nanoparticles (NPs) because their well-defined crystalline structure and monodisperse pore dimensions allow detailed, quantitative probing of the thermodynamics and kinetics of H_2 desorption without the ambiguity associated with amorphous templates. MOFs have the additional advantage that they can serve as "nanoreactors", in which cavity size and chemical functionality can be designed to facilitate a specific reaction chemistry. The MOF topology can likewise be used to control the shape and connectivity of NPs grown inside them, since channel-like (1-D), layered (2-D), or intersecting channel (3-D) structures are known.[19] Reactant and/or product stability can also be tailored by modifying the nature of the organic "linker" groups or by including open metal sites within the MOF secondary building units (SBUs). In the case of $Cu_3(btc)_2$, the enclosed, approximately spherical pores allowed us to access hydride particle sizes of 1 nm or less. The carboxylate linkers and open Cu(II) sites also stabilize the hydride and its decomposition products including, remarkably, the aluminum metal clusters resulting from the one-step decomposition. Unfortunately, this MOF cannot be used for reversibility studies because it decomposes under the high H_2 pressure and elevated temperature required for the rehydrogenation reaction.[7] Although MOFs as templates for metal hydrides have been used previously,[2,7,20,21] there are no reports of reversibility by hydride@MOFs.[22]

Here, we report reversible hydrogen storage by $NaAlH_4$ confined within the pores of catalyst-functionalized MOF-74(Mg), which serves as both a template for forming hydride NPs and a nanoreactor for decomposing and reforming the hydride. The capacity retention by this material is one of the highest achieved to date, with nearly 90% of the initially stored hydrogen still accessible after four desorption/readsorption cycles. We achieved this by melt-infiltrating the hydride into the 1-D channels of MOF-74(Mg), which were preloaded with a titanium catalyst, $TiCl_4$ (referred to hereafter as $NaAlH_4$(Ti)@MOF-74(Mg)). This MOF was selected because it displays remarkable chemical and thermal stability in the presence of both high-pressure H_2 and molten $NaAlH_4$. Additionally, however, MOF-74(Mg) is similar to $Cu_3(btc)_2$ in two key ways that allow direct comparisons between the new results described here and our earlier work. First, it has open metal sites, which could stabilize hydride NP decomposition products and facilitate rehydrogenation by bringing H_2 molecules into close proximity with them. Second, its hexagonal pore dimensions are only slightly larger (12 Å in diameter) than those of $Cu_3(btc)_2$. Like $NaAlH_4$@$Cu_3(btc)_2$, the nanoscale hydride within MOF-74(Mg) exhibits fast hydrogen desorption kinetics *via* a one-step decomposition process. The results suggest that careful tailoring of the pore dimension(s) to enhance interactions of the hydride with the chemical groups comprising the pore and the presence of electron-accepting sites to stabilize the catalyst are necessary to achieve reversibility and maximize capacity retention.

RESULTS

Synthesis and Characterization of As-Synthesized Ti-Doped $NaAlH_4$@MOF-74(Mg). The two-step process by which we synthesized Ti-doped $NaAlH_4$@MOF-74(Mg) yields nanoconfined hydride without observable degradation of the MOF template. As described in detail in the Methods section, the activated MOF is first exposed to gas-phase $TiCl_4$, followed by melt infusion with $NaAlH_4$ at 195 °C under 25 MPa H_2 overpressure. We used an incipient wetness infiltration method, which is designed to avoid

the formation of any residual bulk hydride. The amount of hydride used was less than the amount required to completely fill the MOF-74(Mg) pores, and the 1-D parallel channels in MOF-74 are expected to exhibit capillary effects that will facilitate the hydride infiltration.

We characterized the melt-infiltrated samples by a variety of methods to confirm that the hydride fills the pores of the intact MOF and is not merely a coating on the outside of the particles. The overall atomic composition of the sample is confirmed by elemental analysis, showing that a 21% (m/m) $NaAlH_4$ loading is achieved. Strong evidence that this hydride is located within the MOF pores is obtained first from the powder X-ray diffraction (XRD) pattern of $NaAlH_4$(Ti)@MOF-74(Mg), which is very similar to that of neat, activated MOF-74(Mg) (Figure 1) and agrees with the established MOF-74(Mg) crystal structure.[23] The XRD data for the as-synthesized material exhibit no diffraction peaks from metallic Ti or crystalline $NaAlH_4$, indicating that the hydride has no long-range order. Furthermore, there is no indication that the crystal structure or long-range order of the MOF is reduced, and there are no unassigned reflections that would indicate new MOF phases, decomposition of the hydride, and/or a possible reaction between the MOF host and the hydride.

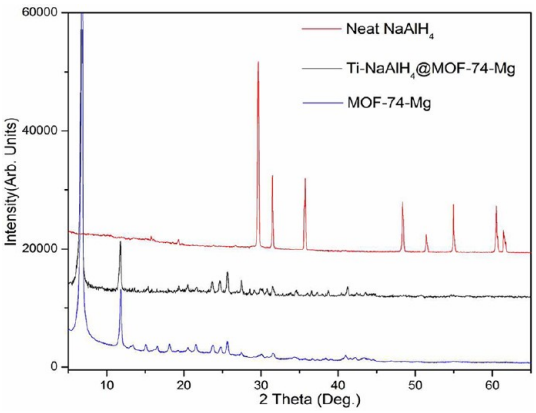

Figure 1. Powder XRD patterns for bulk $NaAlH_4$ and Ti-$NaAlH_4$ melt infiltrated into MOF-74(Mg).

The uniform distribution of the hydride and catalyst throughout the MOF crystals is demonstrated through scanning electron microscopy (SEM) measurements using energy-dispersive spectroscopy (EDS). The penetration depth for 15 keV electrons used here is approximately 5 μm, so this method probes the entire particle and not only its surface. SEM images of a typical infiltrated MOF-74 particle are shown in Figure 2A,B, with the EDS maps corresponding to the area depicted in Figure 2 shown in Figure 2C. A typical EDS scan is shown in Figure 2D and confirms the presence of Na,

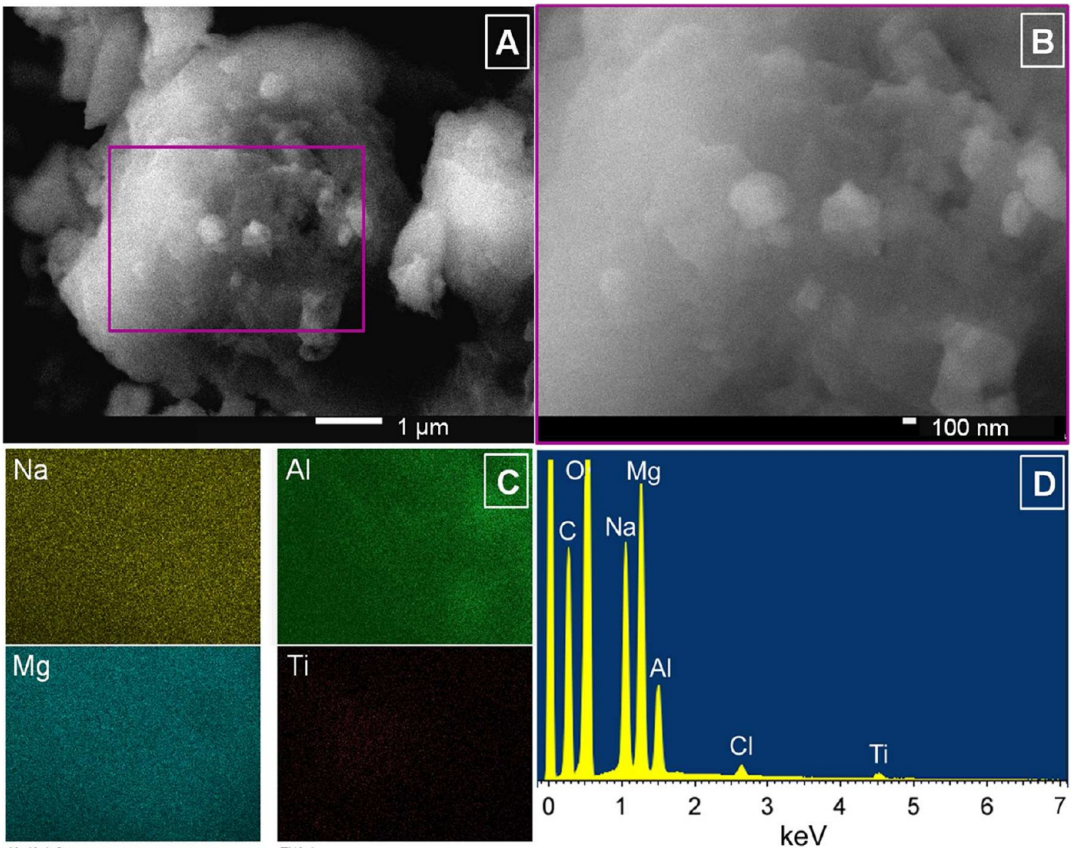

Figure 2. SEM and EDS analysis on $NaAlH_4$(Ti)@MOF-74(Mg). (A) SEM image of an infiltrated MOF-74 particle. (B) SEM image of the area selected for EDS analysis. (C) SEM-EDS elemental mapping images for Na, Al, Mg, and Ti. (D) EDS spectrum of the selected area shown in panel A.

TABLE 1. BET Surface Area Analyzed by Nitrogen Absorption Measurements

sample	BET surface area (m^2/g)	pore volume (cm^3/g)
MOF-74(Mg) activated	1530	0.593
$NaAlH_4$(Ti)@MOF-74(Mg) after melt infiltration	407	0.157
$NaAlH_4$(Ti)@MOF-74(Mg) after 4 cycles	131	0.092

Al, Mg, Ti, and Cl. The elemental maps indicate that Na, Al, Mg, and Ti are dispersed throughout the particle and do not suggest an accumulation of hydride in a particular location or nucleation to form bulk crystals physically mixed with the MOF template.

Fourier transform infrared (FTIR) spectroscopy employed to probe the bulk of the MOF-74(Mg) sample, also shows that the framework is not decomposed upon infiltration and that $NaAlH_4$ is likely present within the MOF pores. The FTIR exhibits a broad shoulder around 1650 cm^{-1} corresponding to the Al−H stretch from the hydride (Figure S1 in Supporting Information). The characteristic bands seen in the spectrum of the activated MOF ($\nu_{as}(CO_2^-)$) appear at 1589 cm^{-1}, while the symmetric stretching vibration $\nu_s(CO_2^-)$, detected at 1416 cm^{-1}, remains essentially unchanged upon infiltration with $TiCl_4$ and $NaAlH_4$. As the asymmetric and symmetric bands of the carboxylate groups are known to be very sensitive to the coordination environment, the lack of any significant changes in these bands upon infiltration with $TiCl_4$ and $NaAlH_4$ indicates that MOF-74(Mg) is unaffected by the infiltration process. These results are consistent with the XRD data, which indicate that the framework structure is preserved. The samples remain porous after infiltration (see Table 1), in spite of the relatively high hydride loading. The as-activated MOF-74(Mg) displays a N_2 BET surface area of 1530 m^2/g and a pore volume of 0.593 cm^3/g. After loading with $TiCl_4$ and $NaAlH_4$, the surface area decreases to 407 m^2/g, while the pore volume reaches 0.157 cm^3/g. These results are consistent with previous reports showing that the MOF surface area decreases after infiltration with guest molecules.[24]

Together, these data indicate that $NaAlH_4$ penetrates the MOF pores and do not support the notion that any significant quantity of hydride exists on the outer surfaces of the particles. Since the external surface area of the MOF powder is extremely low (essentially zero by comparison with the interior surface area), an external coating would of necessity be very thick at our hydride loadings. For a 5 μm particle, such as is shown in Figure 2, and noting the densities of MOF-74(Mg) and $NaAlH_4$ (1.51 and 0.91 g cm^{-3}, respectively), we estimate the average thickness of a hydride coating on the particle surface to be ~780 nm. Since no evidence of an amorphous $NaAlH_4$ bulk phase has ever been reported as a result of infiltrating nanoporous templates, it is reasonable to expect that a surface coating would be crystalline, which is not consistent with the XRD data described above.

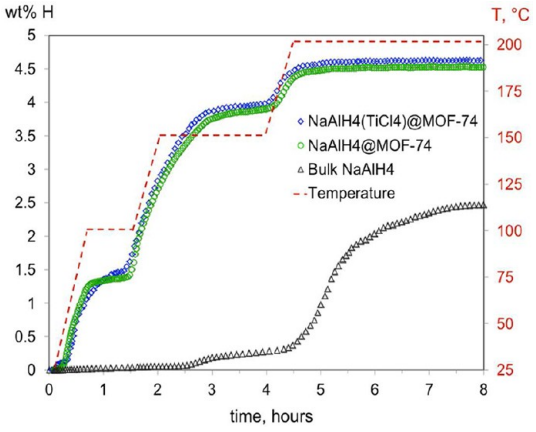

Figure 3. Temperature-programmed desorption spectra for bulk $NaAlH_4$ compared with catalyzed and uncatalyzed $NaAlH_4$@MOF-74(Mg). The wt % H values are normalized to the $NaAlH_4$ loading.

Gas Desorption. Residual gas analysis (RGA) demonstrates that almost no H_2 is desorbed by the activated form of MOF-74(Mg), as seen in Figure S2 (Supporting Information). In contrast, the RGA of the $NaAlH_4$(Ti)-@MOF-74(Mg) sample shows that H_2 is the primary gas evolved, with only traces of H_2O (*m/z* 18), MeOH (*m/z* 32), CO_2 (*m/z* 44), and DMF (*m/z* 73) detected. The CO_2 signal begins to increase only at temperatures above ~300 °C, indicating that the MOF-74(Mg) template is stable throughout the temperature range of the desorption experiments. Thermogravimetric/mass spectrometry (TGA/MS) analysis reveals that H_2 desorption occurs in the 50−250 °C range, while the decomposition of the MOF starts >250 °C (Figure S3, Supporting Information). This was quantified using temperature-programmed desorption (TPD), which demonstrates that confining the hydride in MOF-74(Mg) leads to significant destabilization, consistent with what is observed when $NaAlH_4$ is confined in $Cu_3(btc)_2$.[7] As seen in Figure 3, the bulk $NaAlH_4$ control sample undergoes essentially no dehydrogenation until the temperature reaches 150 °C, while the uncatalyzed and Ti-catalyzed $NaAlH_4$@MOF-74(Mg) samples have already lost ~65% of the theoretically possible hydrogen at 2.5 h and 150 °C. These desorbed wt % hydrogen values were normalized to reflect the weight of $NaAlH_4$, assuming 21 wt % loading of $NaAlH_4$ in the pores of MOF-74(Mg). The dehydrogenation of the bulk $NaAlH_4$ sample begins at 150 °C, and even after 8 h at 200 °C, less than 2.5 wt % hydrogen is desorbed. In contrast, the onset temperature for dehydrogenation by undoped $NaAlH_4$@MOF-74(Mg) is at ~50 °C and reaches a maximum value of 4.5 wt % at 200 °C. This corresponds to nearly complete dehydrogenation of $NaAlH_4$ to NaH (maximum theoretical H_2 capacity is 5.6 wt %). In contrast, after heating to 200 °C, the extent of desorption from a bulk sample is <50%.

This suggests that the catalyst has little or no role in the desorption of $NaAlH_4$, which is another considerable difference in behavior relative to bulk hydride. It also contrasts with the previous work by Nielsen *et al.*, who observed a reduction in the onset of H_2 desorption by a $NaAlH_4$-infiltrated porous carbon preloaded with $TiCl_3$ catalyst.[1] Hydrogen desorption from the bulk requires titanium or other transition-metal catalyst to bring the desorption temperature to below 150 °C.[13,25]

We quantified the $NaAlH_4$(Ti)@MOF-74(Mg) desorption kinetics by measuring the H_2 evolution rate under isothermal conditions. Samples were decomposed in a PCT instrument, using a calibrated volume and temperatures ranging from 150 to 195 °C. The quantity of desorbed hydrogen (in wt %) *versus* time (in min) was monitored and is depicted in Figure 4 for each temperature. Since the desorption reactions were performed at temperatures below 200 °C, the amounts of hydrogen produced are less than expected on the basis of TPD results shown in Figure 3. The data clearly show, however, that the H_2 desorption process is thermally activated. The fit of these data to the Arrhenius equation (inset of Figure 4) yields 57.4 ± 2.4 kJ mol^{-1} for the desorption activation energy for $E_a(d)$ of $NaAlH_4$(Ti)@MOF-74(Mg), which is considerably lower than the value reported for bulk Ti-catalyzed $NaAlH_4$,[26] that is, 79.5 kJ mol^{-1} (Table 2).

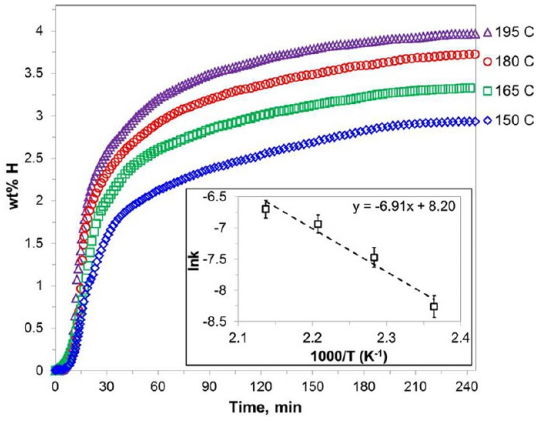

Figure 4. Isothermal desorption of $NaAlH_4$(Ti)@MOF-74(Mg) at 150, 165, 180, and 195 °C. The inset shows the Arrhenius plot at these temperatures. The wt % H values are normalized to the $NaAlH_4$ loading.

TABLE 2. Measured Activation Energies for Bulk $NaAlH_4$ and Nanoconfined $NaAlH_4$

Ti (mol %)	H_2 capacity (% M/M)	$E_a(d)$ (kJ mol^{-1})	ref
0 (bulk)	5.12	118.1	26
2% (bulk)	4.25	79.5	26
0 (10 nm pores)		58	3
0 (4 nm)		46	4
0 (1 nm)		53.3	7
3 (≤1.2 nm)	4.2	57.4	this work

Reversibility of Nanoconfined $NaAlH_4$. A series of charge/discharge experiments using the PCT apparatus demonstrate that the kinetic enhancements described above are preserved over several cycles. We find that the undoped $NaAlH_4$@MOF-74(Mg) displays limited reversibility (<2.0 wt % at 160 °C under 10.5 MPa hydrogen; see Figure S4, Supporting Information). In contrast, the $NaAlH_4$(Ti)@MOF-74(Mg) samples were cycled through four dehydrogenation/rehydrogenation sequences that display minimal capacity losses. Plots of the desorbed hydrogen weight percentage as a function of temperature are shown in Figure 5. After each dehydrogenation cycle (~4 h), the samples were rehydrogenated by heating to 160 °C under 10.5 MPa H_2 pressure for 2 h, then gradually cooled to room temperature under H_2 pressure. The first dehydrogenation cycle releases 4.1 wt % hydrogen, after which the capacity decreases to 3.9, 3.7, and 3.6 wt % for the second, third, and fourth cycles, respectively. In addition, the rehydrogenation reaction is faster than bulk Ti-doped material, where absorption to 95% capacity takes over 1 h at 2 mol % and about 0.5 h at 4 mol % Ti doping.[26] In contrast, $NaAlH_4$(Ti)@MOF-74(Mg) samples are saturated with hydrogen in less than 20 min

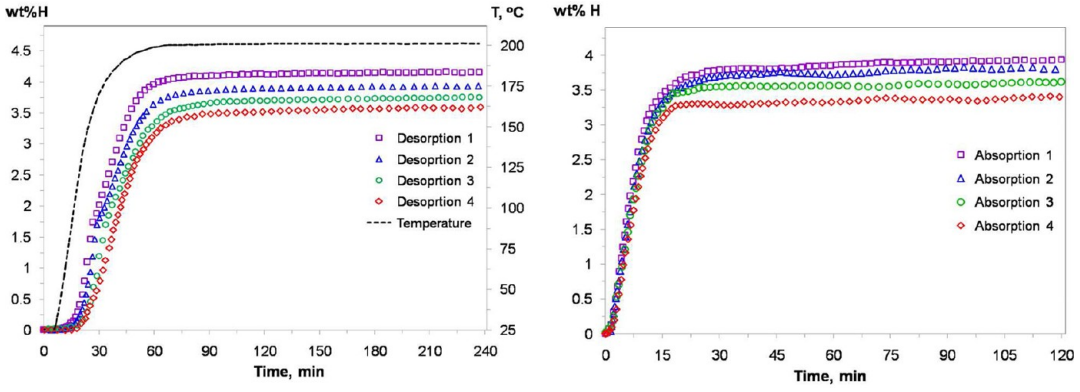

Figure 5. Desorption (left) and absorption (right) of $NaAlH_4$(Ti)@MOF-74(Mg) for four consecutive cycles. The dehydrogenation was done upon heating from room temperature to 200 °C, while the rehydrogenation was done at 160 °C under 10.5 MPa H_2 pressure. The wt % H values are normalized to the $NaAlH_4$ loading.

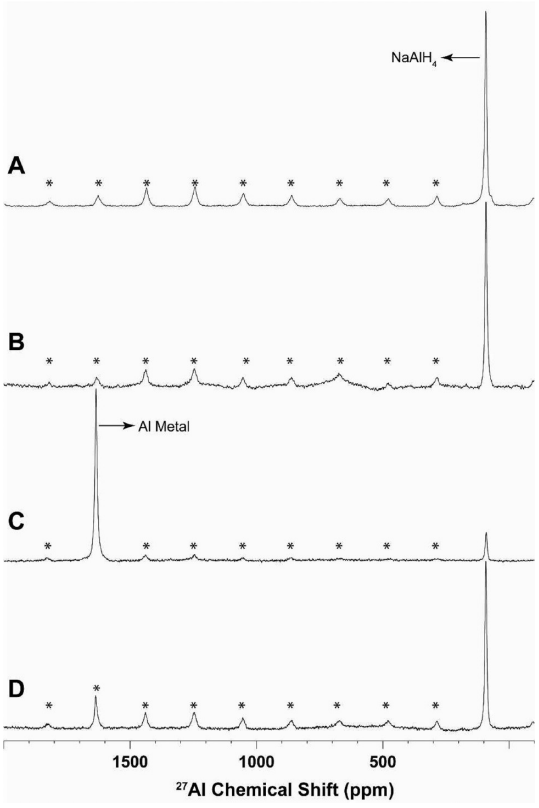

Figure 6. ^{27}Al NMR spectra for (A) neat $NaAlH_4$, (B) $NaAlH_4$-(Ti)@MOF-74(Mg), (C) desorbed $NaAlH_4$(Ti)@MOF-74(Mg) after 4 dehydrogenation cycles, and (D) $NaAlH_4$(Ti)@MOF-74(Mg) after H_2 absorption (after 4 desorption/absorption cycles). Spinning side bands are indicated by stars.

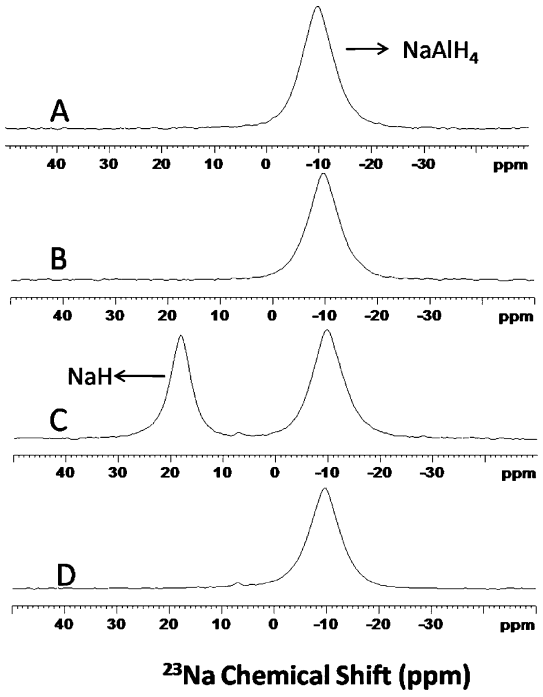

Figure 7. ^{23}Na NMR spectra for (A) neat $NaAlH_4$, (B) $NaAlH_4$-(Ti)@MOF-74(Mg), (C) sample of (B) after four H_2 desorption cycles, showing the formation of NaH, and (D) sample of (C) after H_2 reabsorption showing regeneration of $NaAlH_4$.

under the above-mentioned conditions. Also, a two-step reaction is clearly evident in the bulk absorption profiles of Sandrock *et al.* (see Figure 1 in ref 26). Our absorption profiles show no similar break and suggest a one-step reaction. Finally, the capacity changes observed in $NaAlH_4$(Ti)@MOF-74(Mg) are far smaller than occur in either bulk $NaAlH_4$[7] or the hydride confined within carbon aerogels; the capacity of the latter drops by 50% after four cycles.[1] Note that neither the FTIR (Figure S1, Supporting Information) nor the XRD pattern (Figure S5, Supporting Information) indicate that any significant decomposition of the MOF occurs. The decrease in the surface area (131 m^2/g) and pore volume (0.092 cm^3/g) of the cycled sample is most likely the result of some migration of material toward the outer surface of the crystals that hinders access of N_2 to the MOF interior.

Characterization of $NaAlH_4$(Ti)@MOF-74(Mg) Using Solid-State NMR. Solid-state NMR spectra confirm the presence of the hydride in the infiltrated MOF-74(Mg) sample and show that the desorption and rehydrogenation reactions occur without formation of intermediate phases. ^{27}Al and ^{23}Na NMR spectra are shown in Figures 6 and 7, respectively, and the observed resonances are summarized in Table 3. The spectra from both nuclei for $NaAlH_4$(Ti)@MOF-74(Mg) are nearly identical to those of the neat (bulk) material. In the infiltrated sample, the ^{27}Al resonance occurs at δ = 95.2 ppm and the ^{23}Na signal is at $\delta = -9.6$ ppm, while in the bulk material, they are at δ = 95.6 and -9.6 ppm, respectively, consistent with a previous report.[27] These observations suggest that the bonding in $NaAlH_4$ is not greatly changed by melt infiltration of the MOF pores. The spectra also display no signals corresponding to Al metal, Al_2O_3, or Na_3AlH_6, showing that the infiltrated $NaAlH_4$ does not react with the framework under the high H_2 pressure and temperature required for melt infiltration.

Spectra obtained from a dehydrogenated sample after four dehydrogenations, shown in Figures 6C, 7C, and S6, reveal the nature of the decomposition products. A very large (>80%) signal is observed at $\delta = +1637$ ppm corresponding to Al metal (Figure 5B), along with a minor resonance (<1%) at $\delta = -43$ ppm corresponding to a small amount of Na_3AlH_6 evidently formed as a decomposition product (expanded spectrum in Figure S6C, Supporting Information). There is also resonance at δ = 95.6 ppm corresponding to unreacted $NaAlH_4$. The ^{23}Na spectrum shows two major resonances at $\delta = -9.6$ ppm, assigned to unreacted $NaAlH_4$, and $\delta = +18.2$ ppm, corresponding to NaH. Both are consistent with reported literature values.[27] However, the $NaAlH_4$/NaH molar ratio, inferred from the ratio of the corresponding resonances in Figure 7C, is not consistent with the corresponding $NaAlH_4$/Al ratio taken from the ^{27}Al MAS NMR spectrum (Figure 6C), suggesting that there may be another Na species

TABLE 3. Positions of NMR Chemical Shifts (in ppm) of the Phases Detected in $NaAlH_4$(Ti)@MOF-74(Mg) at Different Stages of the Reaction

compound	^{23}Na	assignment	^{27}Al	assignment
pure $NaAlH_4$	−9.6	$NaAlH_4$	95.6	$NaAlH_4$
infiltrated Ti-doped $NaAlH_4$@MOF-74(Mg)	−9.6	$NaAlH_4$	95.2	$NaAlH_4$
H_2 desorbed Ti-doped $NaAlH_4$@MOF-74(Mg)	−9.6	unreacted $NaAlH_4$ (60%)	1637 (88%)	Al metal
	18.2	NaH (40%)	95.6 (12%)	unreacted $NaAlH_4$
			−43 (<1%)	Na_3AlH_6
reabsorbed Ti-doped $NaAlH_4$@MOF-74(Mg)	−9.6	$NaAlH_4$	1637 (20%)	Al metal
			95.2 (80%)	$NaAlH_4$

present. In particular, we cannot rule out the presence of metallic sodium, which displays a chemical shift (+1123 ppm) and lies outside of the tested ^{23}Na spectral window. In addition, the ^{23}Na MAS NMR spectrum of the nanoconfined hydride sample displays a minor resonance at +7.1 ppm that is assigned to NaCl (Figures 7B−D and S7) and which likely originates from the reaction of $TiCl_4$ with $NaAlH_4$. Following H_2 reabsorption, the majority of the Al metal signal ($\delta = +1637$ ppm) disappears and the δ = 95.6 ppm signal reappears, indicating that the Al metal is converted to $NaAlH_4$ (Figure 6D). This is corroborated by the ^{23}Na spectrum (Figure 7D), which exhibits a major signal at $\delta = -9.6$ ppm corresponding to $NaAlH_4$. These results clearly show that most of the Al metal is converted to $NaAlH_4$ after rehydriding, as is the NaH product.

DISCUSSION

Although there are now many examples in the literature showing that nanoconfinement dramatically improves hydride desorption kinetics, it is clear that this represents only half of the equation: reversibility is also required to achieve a successful storage material. The results presented here demonstrate that both accelerated H_2 desorption kinetics and reversibility can be achieved by confining $NaAlH_4$ within a nanoporous support. Because of the well-defined, uniform pore dimensions and chemical environment associated with the MOF-74 template, it is possible to establish why these favorable properties are achieved with a much greater degree of confidence than is feasible with disordered templates such as porous carbons. As a result, some basic features of an optimal template for reversible storage can be identified that can assist in future development of nanohydride storage materials.

We first consider the desorption process. On the basis of our prior results for infiltrated MOFs[2,7] and those of others cited above, we conclude that the scaffold pore size must be less than 20 nm, and probably much smaller (perhaps as much as a factor of 10), to obtain desorption activation energies $E_a(d) < 60$ kJ (mol H_2)$^{-1}$. Both MOF-74 and $Cu_3(btc)_2$[2,7] templates, which have pores in the 1.0−1.3 nm range, kinetically destabilize $NaAlH_4$ to this extent. The results of Baldé *et al.* ($NaAlH_4$ stabilized on carbon nanofibers[28]) are consistent with this conclusion, indicating that particles in the 2−10 nm size range have a desorption activation energy of 58 kJ (mol H_2)$^{-1}$. This value is quite similar to those we obtain using MOFs with much smaller pores (Table 2). However, the relatively broad particle size distribution makes it difficult to determine whether particles ≥10 nm are kinetically destabilized to the same extent as 1.0 nm particles. Related work by Li *et al.*[4] and Nielsen *et al.*[1] using 4 nm mesoporous carbon (MPC) and carbon aerogel having an average pore size of 17 nm, respectively, achieved increases in desorption rates comparable to what we observe. However, in both cases, the presence of nanocrystalline hydride that is much larger than the template pores (~35 nm based on the Scherer formula) makes it unclear whether the observed rate increase is due to hydride within the pores or on template surfaces. As a result, the use of the MOF-74 template, with its monodisperse pore size, provides the most conclusive results to date concerning the effect of size on hydrogen desorption kinetics.

The titanium catalyst evidently plays no role in the improved desorption kinetics, as our results show virtually identical desorption curves for catalyzed and uncatalyzed $NaAlH_4$@MOF-74(Mg) (Figure 3). This strongly contrasts with bulk hydride, where both desorption and regeneration require a catalyst to proceed at reasonable rates above 150 °C.[25,26,29−31] We previously suggested that reduced $NaAlH_4$ desorption activation energies are primarily due to the reduction in particle size, rather than a chemically specific interaction with scaffold pore walls. This hypothesis is supported by the fact that $NaAlH_4$ confined within MOF pores[2,7] and supported on various carbons[1,5,12] decomposes *via* a one-step decomposition pathway with similar activation energies, even though we expect that these templates have rather different surface chemistries. This is consistent with DFT calculations, as well.[14,15] Although there is evidence that the surfaces of porous carbons are highly defected and can be terminated in carboxylate and hydroxyl groups,[32,33] functionalities present in the linkers composing our MOF templates, such groups are nevertheless bound to a highly conjugated, graphite-like surface. This surface is therefore quite different from the single phenyl rings comprising the linkers of MOF-74(Mg) and $Cu_3(btc)_2$.

The reversibility of $NaAlH_4$(Ti)@MOF-74(Mg) with minimal capacity loss upon cycling indicates that the

chemical environment of the MOF-74 pore plays a significant role in immobilizing $NaAlH_4$ decomposition products and/or the titanium catalyst, leading us to draw comparisons with the behavior of $NaAlH_4$ supported on carbon templates. The most direct comparison is with the work of Nielsen *et al.*, in which $NaAlH_4$ was supported on MPC containing a Ti catalyst.[1] In this case, the reversibility was limited (>50% capacity loss after 4 cycles), possibly due to agglomeration of the Al and NaH decomposition products or loss of catalyst during thermal cycling. In contrast, the presence of both positive and negatively charged groups within the MOF-74 pore should stabilize the hydride decomposition products and limit their mobility. XRD patterns of the desorbed $NaAlH_4$@MOF samples show no evidence of crystalline Al, although NMR shows that metallic aluminum is clearly present. In contrast, XRD shows that infiltrating MPC[1,16] and carbon aerogel[4] with $NaAlH_4$ produces crystalline metallic Al, which may serve as a nucleation site for product formed during desorption. If formed, bulk aluminum can reduce the reversibility of the material, as it requires high H_2 pressures for complete rehydrogenation.[34] Recent results by Xiong *et al.* on nano-$NaAlH_4$ confined inside Ti-loaded MPC[16] seem to support this hypothesis, as bulk Al was detected by XRD after both dehydrogenation and rehydrogenation steps.

Similarly, the open Mg^{2+} coordination sites of MOF-74(Mg) can coordinate to either $TiCl_x$ through a chlorine atom or to a titanium metal cluster to reduce loss of catalyst. Our results are not sufficient to determine the stoichiometry of the catalyst within MOF-74(Mg), but NMR evidence suggests that some loss of Cl occurs *via* a metathesis reaction with the hydride to form NaCl (Figure S7, Supporting Information). Thus, both $TiCl_x$ and $(Ti)_n$ clusters are possible. Extensive literature concerning Ziegler–Natta catalysts shows that $TiCl_x$ species (including $TiCl_4$) can be stabilized on four- and five-coordinate Mg^{2+} ions located on the surface, edges, and other defect sites of the typically used $MgCl_2$ support.[35] The very light catalyst loading in our materials (~0.6 wt %) may also contribute to greater reversibility. Assuming the catalyst occupies an exchangeable position at the framework Mg^{2+} and that there is no more than one Ti atom per Mg^{2+}, then on average there are no more than ~1 Ti atom per 50 Mg^{2+}. Since six Mg^{2+} form a hexagonal ring in the MOF-74(Mg) pore, this means that there is only one Ti atom every eighth or ninth Mg_6 hexagon. This large separation, combined with potentially strong chemical bonding to Mg, will likely inhibit Ti diffusion to a much greater extent than in MPC.

As indicated by the BET data in Table 1, much of the MOF pore volume must be occupied by $NaAlH_4$ after infiltration. It is therefore logical to expect that there exist extended regions of the pores that are completely filled by hydride. However, it is also possible that

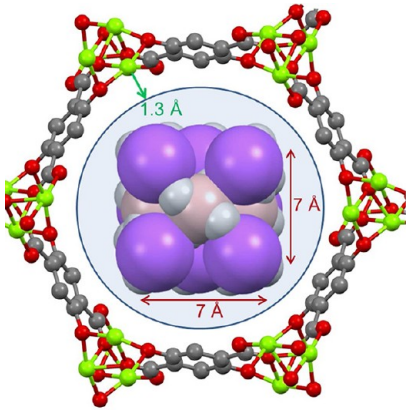

Figure 8. Schematic representation of the $(NaAlH_4)_8$ clusters inside the MOF-74(Mg) pores. The space inside the sphere corresponds to the available space outside of magnesium van der Waals radius (1.3 Å; see ref 38).

$NaAlH_4$ within the MOF-74(Mg) pores consists of clusters having very few, if any, atoms that do not interact with the pore surfaces. It is well-known that, at the nanoscale, the thermodynamic properties of metal hydride particles are influenced by their surface energy.[6,36] As noted in other nanoconfined cluster systems, atoms in the interior of a cluster are more highly coordinated and are therefore more stable than those at the cluster surface.[37] Although the exact molecular-level decomposition mechanism of the nanoclusters is difficult to determine, it is plausible that the dehydrogenation products lie on or near the molecular "surfaces" of the pores. In our previous investigation of $NaAlH_4$ confined within the MOF $Cu_3(btc)_2$, the average hydride cluster was estimated to have eight formula units.[7] Clusters of this size can easily fit within the pore volume defined by the van der Waals radii[38] in the MOF-74(Mg) pore, as seen in Figure 8. The first-principles relaxed cluster geometry for $(NaAlH_4)_8$ is a rectangular parallelepiped consisting of four stacked square layers in which $[AlH_4]^-$ and Na^+ are on opposing corners. Adjacent 2-formula unit layers are rotated by 90° with respect to each other to allow the corner charges to alternate in sign. (Details of the cluster geometry may be found in ref 14, while more extensive discussion of ionic nanocluster geometries may be found elsewhere.[39]) Thus, for destabilized clusters located on or near the pore surfaces, lower desorption temperatures and reduced H_2 rehydrogenation pressures would be expected. Given the high loading achieved here, it is possible that these clusters are chemically linked in some way, creating a chain of clusters within the 1-D channels of MOF-74(Mg). While admittedly speculative, this explanation is consistent with the highly accelerated H_2 desorption kinetics that are observed.

The extent to which these non-bulk-like properties can be maintained will determine the extent of reversibility. In our materials, a comparison of the XRD

patterns of the cycled $NaAlH_4$(Ti)@MOF-74(Mg) with as-synthesized MOF-74(Mg) shows virtually no difference in the long-range order of the framework material (Figure S5, Supporting Information). The cycled material does show evidence in XRD of one or more minor crystalline phases. The most prominent peaks at 32.5, 32.9, and 33.6 2θ indicate a minor amount of Na_3AlH_6 (a fourth peak at 39.8° 2θ cannot be assigned), which is consistent with the ^{27}Al MAS results shown in Figure S6 (Supporting Information). This phase is also observed upon aging the $NaAlH_4$(Ti)@MOF-74(Mg) material for 42 days at 190 °C under H_2 pressure (Figure S8, Supporting Information). Na_3AlH_6 could be formed by decomposition of trace amounts of the hydride located outside the MOF pores. Using the full width at half-maximum (fwhm) of the two strongest Na_3AlH_6 peaks in the XRD in Figure S8 (Supporting Information), an average coherence length of 750 Å obtained from the Debye–Scherrer equation is an approximate lower bound on the particle size. This implies that the minor Na_3AlH_6 phase is external to the pores of the MOF.

CONCLUSIONS

The results presented here show that both fast desorption kinetics and an exceptionally high degree of reversibility can be achieved by confining $NaAlH_4$ within the well-ordered pores of a MOF template. This performance is evidently the result of specific chemical and structural features of the MOF template that are distinct from others used to date. In particular, these are (1) pore dimensions that allow a majority of the hydride to be in close contact with the pore walls; (2) open metal sites that can coordinate and stabilize the Ti catalyst; and (3) both positive and negatively charged atoms that can stabilize the decomposition products, preventing diffusion and agglomeration. Using this knowledge, it may be possible to design other templates composed of economical materials (functionalized porous carbons or metal oxide aerogels, for example) that have high thermal stability as well as the pore volume needed to achieve an acceptable hydride loading.

Regarding the question of which is the dominant factor in determining the overall desorption behavior, hydride nanocluster size or the chemical properties of pore, our results support the concept that size and/or the act of confining the hydride is the key. Our results are fully consistent with our previous report of $NaAlH_4$ confined within $Cu_3(btc)_2$, a MOF with very similar pore dimensions and environment. Additionally, the trend in H_2 activation energy with pore size, defined by both our results and those of previous investigators using porous carbon templates,[4−6] is maintained, as is the one-step decomposition mechanism predicted by theory[14,15] and demonstrated using various nanoporous templates.[5−7,12] However, the best evidence to date that particle size is the dominant factor is the similarity of both mechanism and activation barrier for H_2 desorption from nanoscale $NaAlH_4$ across a range of different support materials. If particle size is *not* the dominant factor, then these similar results involving diverse materials suggest that a rather nonspecific interaction with pore walls is all that is necessary to lower the desorption activation barrier. In our view, this is encouraging because it should make it easier to design porous materials with the desired features listed above.

Finally, these results support the concept of a chemical "nanoreactor" as an important tool for altering and controlling both kinetics and thermodynamics of chemical processes. In many ways, MOFs are ideal for this purpose, with their regular pore dimensions and potential to be functionalized with chemical groups to facilitate specific chemical reactions (a concept that has been recently reviewed in the context of catalysis[40]). We hope that this work will lay the groundwork for future investigations that will allow identification of more advanced porous nanoreactors to realize the full potential of the reversible nanoconfined metal hydrides. More broadly, we envision a wide range of uses for these structures to address important problems within the emerging areas of nanostructured materials for energy generation and storage.

METHODS

Synthesis and Activation of MOF-74(Mg). The MOF-74(Mg) material studied in this work was synthesized from a solvothermal reaction of 2,5-dihydroxyterephthalic acid (98%, from Aldrich) with magnesium nitrate (99%, Aldrich) in a mixture of *N*,*N*-dimethylformamide (DMF) (99%, Acros), absolute ethanol (99.5%, Aldrich), and deionized water following a previously reported procedure.[23] $Mg(NO_3)_2 \cdot 6H_2O$ (0.712 g, 2.78 mmol) and 2,5-dihydroxyterephthalic acid (0.167 g, 0.84 mmol) were dissolved under sonication in a 15:1:1 (v/v/v) mixture of DMF (67.5 mL), ethanol (4.5 mL), and water (4.5 mL). The homogeneous solution was then transferred to a 125 mL Teflon-lined stainless steel autoclave. The autoclave was capped tightly and heated to 125 °C in an oven. After 26 h, the autoclave was removed from the oven and yellow microcrystalline material was recovered and repeatedly washed with DMF. The product was then soaked in DMF and heated to 85 °C for 16 h. The solvent was carefully decanted from the product and replaced with methanol. It is critical to fully exchange the solvent with methanol prior to activation in order to achieve high surface areas. Fresh methanol was used for solvent exchange for six times over 3 days. The yellow precipitate was isolated by filtration and washed thoroughly with methanol. The guest molecules incorporated in the crystals were removed under a dynamic vacuum at 200 °C for 16 h, yielding a yellow crystalline material.

Hydride Melt Infiltration. $TiCl_4$ and $NaAlH_4$ were loaded into the pores of MOF-74(Mg) using a two-step infiltration technique. First, the as-activated MOF-74(Mg) was infiltrated with $TiCl_4$ vapors for 16 h at 100 °C. Next, a mixture of $NaAlH_4$ and $TiCl_4$@MOF-74(Mg) in a 1:4 weight ratio was ground together in an Ar-filled glovebox. The material was then loaded and sealed in a stainless steel autoclave. The sealed autoclave was evacuated and refilled to 25 MPa H_2 to avoid the decomposition of

$NaAlH_4$ upon heating. Then, the autoclave was heated to 195 °C and kept at that temperature for 2 h. During the process, $NaAlH_4$ melts and infiltrates into the MOF-74(Mg) pores. The sample was cooled to room temperature under hydrogen pressure to minimize H_2 desorption. The sample obtained after impregnation will be referred to hereafter as $NaAlH_4$(Ti)@MOF-74(Mg). Elemental analysis of the $NaAlH_4$(Ti)@MOF-74(Mg) sample indicated a 21% (m/m) $NaAlH_4$ loading, while the total titanium content in the nanocomposite was 0.58 wt %. This corresponds to 3.1 mol % titanium doping of the hydride.

Hydrogen Desorption and Hydride Regeneration. We used thermal gravimetry/mass spectroscopy analysis (TGA-MS) to analyze the evolved gas species upon heating. The hydride@MOF samples were analyzed on a Mettler Toledo TGA system coupled to a Pfeiffer mass spectrometer under a continuous flow of ultrahigh purity Ar to avoid oxidation during the runs. Samples were heated from ambient temperature to 500 °C at a heating rate of 5 °C/min. The mass spectra of the evolved species were measured in the *m/z* range of 1 to 200 mass units. The extent of pore filling was determined by nitrogen physisorption using a Quadrasorb SI surface area analyzer (Quantachrome). Powder X-ray diffraction (XRD) patterns were collected with a PANalytical Empyrean diffractometer equipped with a PIXcel^{3D} detector and operated at 45 kV and 40 kA using Cu Kα radiation (λ = 1.5418 Å). Scanning electron microscopy (SEM) and energy-dispersive spectroscopy (EDS) were performed on a JSM-7600F thermal emission scanning electron microscope equipped with an Oxford X-Max detector and operated at 15 kV. Attenuated total reflectance infrared spectra were recorded using a Varian 800 FTIR spectrometer.

The dehydrogenation kinetics experiments were performed using an automated PCT-Pro 2000 apparatus, which allows accurate volumetric determination of the amounts of evolved hydrogen by desorbing into an evacuated calibrated volume. The pressure was monitored with calibrated pressure transducers while the sample was heated and maintained at the desired temperature. Typically, a 0.6 g sample was loaded into a stainless steel autoclave and evacuated. Rapid heating of the sample to a desired temperature was accomplished by wrapping the autoclave in a preheated mantle. All of the dehydrogenation experiments were performed in evacuated volumes, the pressure ranging typically between 0 and a maximum of 0.1 MPa. For rehydrogenation, samples were heated to 160 °C under 10.5 MPa H_2 pressure for 2 h. For the purpose of calculations, the MOF-74(Mg) masses were excluded from the determination of the hydrogen amount released from the samples.

All MAS NMR spectra were obtained on a Bruker Avance III 600 instrument operating at 600.13, 156.38, and 158.75 MHz, for ^{1}H, ^{27}Al, and ^{23}Na, respectively. Approximately, 10 mg of sample was used in a 2.5 mm broad-band MAS NMR probe at a spinning speed of 30 kHz under N_2. The samples were run at a set temperature of 298 K, corresponding to a sample temperature of 332 K due to frictional heating from the high-speed spinning. This frictional heating was calibrated previously using the chemical shift variation of $Pb(NO_3)_2$ as an internal thermometer. The ^{1}H MAS NMR spectra were obtained using a rotor-synchronized Hahn echo, while the ^{27}Al and ^{23}Na MAS NMR spectra utilized a single pulse Bloch decay, with ^{1}H TMMP decoupling. The ^{27}Al and ^{23}Na experiments used a $\pi/6$ excitation pulse (83 kHz rf excitation strength) to improve quantification. The ^{1}H NMR chemical shifts were referenced to the external secondary reference adamantane $\delta = +1.38$ ppm with respect to TMS $\delta = 0.0$ ppm, while the ^{27}Al NMR chemical shifts where referenced to external 1 M $Al(NO_3)_3$, $\delta = 0.0$ ppm, and the ^{23}Na NMR chemical shift referenced to external 1 M NaCl, $\delta = 0.0$ ppm. Spectral deconvolutions were performed using the DMFIT software package.[41]

Conflict of Interest: The authors declare no competing financial interest.

Acknowledgment. The authors acknowledge Dr. John Perry for assisting in the synthesis of MOF-74(Mg), and Jeffrey Chames for obtaining SEM/EDX data. We also thank Dr. Sean Maharrey for helpful discussions. This work was funded by the U.S. DOE Hydrogen, Fuel Cells, and Infrastructure Technologies Program. Sandia National Laboratories is a multiprogram laboratory managed and operated by Sandia Corporation, a wholly owned subsidiary of Lockheed Martin Corporation, for the U.S. Department of Energy's National Nuclear Security Administration under contract DE-AC04-94AL85000.

Supporting Information Available: Additional mass spectrometry, residual gas analysis, MAS NMR, FTIR, and XRD data. This material is available free of charge *via* the Internet at http://pubs.acs.org.

REFERENCES AND NOTES

1. Nielsen, T. K.; Polanski, M.; Zasada, D.; Javadian, P.; Besenbacher, F.; Bystrzycki, J.; Skibsted, J.; Jensen, T. R. Improved Hydrogen Storage Kinetics of Nanoconfined $NaAlH_4$ Catalyzed with $TiCl_3$ Nanoparticles. *ACS Nano* **2011**, *5*, 4056–4064.
2. Bhakta, R. K.; Herberg, J. L.; Jacobs, B.; Highley, A.; Behrens, R.; Ockwig, N. W.; Greathouse, J. A.; Allendorf, M. D. Metal−Organic Frameworks as Templates for Nanoscale $NaAlH_4$. *J. Am. Chem. Soc.* **2009**, *131*, 13198–13199.
3. Baldé, C. P.; Hereijgers, B. P. C.; Bitter, J. H.; de Jong, K. P. Sodium Alanate Nanoparticles—Linking Size to Hydrogen Storage Properties. *J. Am. Chem. Soc.* **2008**, *130*, 6761–6765.
4. Li, Y.; Zhou, G.; Fang, F.; Yu, X.; Zhang, Q.; Ouyang, L.; Zhu, M.; Sun, D. De-/Rehydrogenation Features of $NaAlH_4$ Confined Exclusively in Nanopores. *Acta Mater.* **2011**, *59*, 1829–1838.
5. Gao, J.; Adelhelm, P.; Verkuijlen, M. H. W.; Rongeat, C.; Herrich, M.; van Bentum, P. J. M.; Gutfleisch, O.; Kentgens, A. P. M.; de Jong, K. P.; de Jongh, P. E. Confinement of $NaAlH_4$ in Nanoporous Carbon: Impact on H_2 Release, Reversibility, and Thermodynamics. *J. Phys. Chem. C* **2010**, *114*, 4675–4682.
6. Lohstroh, W.; Roth, A.; Hahn, H.; Fichtner, M. Thermodynamic Effects in Nanoscale $NaAlH_4$. *ChemPhysChem* **2010**, *11*, 789–792.
7. Bhakta, R.; Maharrey, S.; Stavila, V.; Highley, A.; Alam, T.; Majzoub, E.; Allendorf, M. Thermodynamics and Kinetics of $NaAlH_4$ Nanocluster Decomposition. *Phys. Chem. Chem. Phys.* **2012**, *14*, 8160–8169.
8. Adelhelm, P.; Gao, J.; Verkuijlen, M. H. W.; Rongeat, C.; Herrich, M.; van Bentum, P. J. M.; Gutfleisch, O.; Kentgens, A. P. M.; de Jong, K. P.; de Jongh, P. E. Comprehensive Study of Melt Infiltration for the Synthesis of $NaAlH_4$/C Nanocomposites. *Chem. Mater.* **2010**, *22*, 2233–2238.
9. Christian, M. L.; Aguey-Zinsou, K.-F. Core-Shell Strategy Leading to High Reversible Hydrogen Storage Capacity for $NaBH_4$. *ACS Nano* **2012**, *6*, 7739.
10. Nielsen, T. K.; Bösenberg, U.; Gosalawit, R.; Dornheim, M.; Cerenius, Y.; Besenbacher, F.; Jensen, T. R. A Reversible Nanoconfined Chemical Reaction. *ACS Nano* **2010**, *4*, 3903–3908.
11. Zhao-Karger, Z.; Hu, J. J.; Roth, A.; Wang, D.; Kubel, C.; Lohstroh, W.; Fichtner, M. Altered Thermodynamic and Kinetic Properties of MgH_2 Infiltrated in Microporous Scaffold. *Chem. Commun.* **2010**, *46*, 8353–8355.
12. Stephens, R. D.; Gross, A. F.; Van Atta, S. L.; Vajo, J. J.; Pinkerton, F. E. The Kinetic Enhancement of Hydrogen Cycling in $NaAlH_4$ by Melt Infusion into Nanoporous Carbon Aerogel. *Nanotechnology* **2009**, *20*, 204018.
13. Bogdanović, B.; Schwickardi, M. Ti-Doped Alkali Metal Aluminium Hydrides as Potential Novel Reversible Hydrogen Storage Materials. *J. Alloys Compd.* **1997**, *253−254*, 1–9.
14. Majzoub, E. H.; Zhou, F.; Ozoliņš, V. First-Principles Calculated Phase Diagram for Nanoclusters in the Na−Al−H System: A Single-Step Decomposition Pathway for $NaAlH_4$. *J. Phys. Chem. C* **2011**, *115*, 2636–2643.
15. Mueller, T.; Ceder, G. Effect of Particle Size on Hydrogen Release from Sodium Alanate Nanoparticles. *ACS Nano* **2010**, *4*, 5647–5656.
16. Xiong, R.; Sang, G.; Yan, X.; Zhang, G.; Ye, X. Improvement of the Hydrogen Storage Kinetics of $NaAlH_4$ with Ti-Loaded High-Ordered Mesoporous Carbons (Ti-OMCs) by Melt Infiltration. *J. Mater. Chem.* **2012**, *22*, 17183–17189.

17. Zheng, S.; Fang, F.; Zhou, G.; Chen, G.; Ouyang, L.; Zhu, M.; Sun, D. Hydrogen Storage Properties of Space-Confined $NaAlH_4$ Nanoparticles in Ordered Mesoporous Silica. *Chem. Mater.* **2008**, *20*, 3954–3958.
18. Pinkerton, F. E. Comparison of Hydrogen Cycling Kinetics in $NaAlH_4$-Carbon Aerogel Composites Synthesized by Melt Infusion or Ball Milling. *J. Alloys Compd.* **2011**, *509*, 8958–8964.
19. Zhou, H. C.; Long, J. R.; Yaghi, O. M. Introduction to Metal−Organic Frameworks. *Chem. Rev.* **2012**, *112*, 673–674.
20. Gadipelli, S.; Ford, J.; Zhou, W.; Wu, H.; Udovic, T. J.; Yildirim, T. Nanoconfinement and Catalytic Dehydrogenation of Ammonia Borane by Magnesium-Metal−Organic-Framework-74. *Chem.—Eur. J.* **2011**, *17*, 6043–6047.
21. Li, Z.; Zhu, G.; Lu, G.; Qiu, S.; Yao, X. Ammonia Borane Confined by a Metal−Organic Framework for Chemical Hydrogen Storage: Enhancing Kinetics and Eliminating Ammonia. *J. Am. Chem. Soc.* **2010**, *132*, 1490–1491.
22. Juan-Alcaniz, J.; Gascon, J.; Kapteijn, F. Metal−Organic Frameworks as Scaffolds for the Encapsulation of Active Species: State of the Art and Future Perspectives. *J. Mater. Chem.* **2012**, *22*, 10102–10118.
23. Caskey, S. R.; Wong-Foy, A. G.; Matzger, A. J. Dramatic Tuning of Carbon Dioxide Uptake *via* Metal Substitution in a Coordination Polymer with Cylindrical Pores. *J. Am. Chem. Soc.* **2008**, *130*, 10870–10871.
24. Meilikhov, M.; Yusenko, K.; Esken, D.; Turner, S.; Van Tendeloo, G.; Fischer, R. A. Metals@MOFs—Loading MOFs with Metal Nanoparticles for Hybrid Functions. *Eur. J. Inorg. Chem.* **2010**, *2010*, 3701–3714.
25. Bogdanović, B.; Brand, R. A.; Marjanovic, A.; Schwickardi, M.; Tolle, J. Metal-Doped Sodium Aluminium Hydrides as Potential New Hydrogen Storage Materials. *J. Alloys Compd.* **2000**, *302*, 36.
26. Sandrock, G.; Gross, K.; Thomas, G. Effect of Ti-Catalyst Content on the Reversible Hydrogen Storage Properties of the Sodium Alanates. *J. Alloys Compd.* **2002**, *339*, 299–308.
27. Bogdanović, B.; Felderhoff, M.; Germann, M.; Härtel, M.; Pommerin, A.; Schüth, F.; Weidenthaler, C.; Zibrowius, B. Investigation of Hydrogen Discharging and Recharging Processes of Ti-Doped $NaAlH_4$ by X-ray Diffraction Analysis (XRD) and Solid-State NMR Spectroscopy. *J. Alloys Compd.* **2003**, *350*, 246–255.
28. Baldé, C. P.; Hereijgers, B. P. C.; Bitter, J. H.; de Jong, K. P. Facilitated Hydrogen Storage in $NaAlH_4$ Supported on Carbon Nanofibers. *Angew. Chem., Int. Ed.* **2006**, *45*, 3501–3503.
29. Balema, V. P.; Balema, L. Missing Pieces of the Puzzle or About Some Unresolved Issues in Solid State Chemistry of Alkali Metal Aluminohydrides. *Phys. Chem. Chem. Phys.* **2005**, *7*, 1310–1314.
30. Gunaydin, H.; Houk, K. N.; Ozoliņš, V. Vacancy-Mediated Dehydrogenation of Sodium Alanate. *Proc. Natl. Acad. Sci. U.S.A.* **2008**, *105*, 3673–3677.
31. Berseth, P. A; Harter, A. G.; Zidan, R.; Blomqvist, A.; C. Araujo, M.; Scheicher, R. H.; Ahuja, R.; Jena, P. Carbon Nanomaterials as Catalysts for Hydrogen Uptake and Release in $NaAlH_4$. *Nano Lett.* **2009**, *9*, 1501–1505.
32. Figueiredo, J. L.; Pereira, M. F. R.; Freitas, M. M. A.; Órfão, J. J. M. Modification of the Surface Chemistry of Activated Carbons. *Carbon* **1999**, *37*, 1379–1389.
33. Rodríguez-Reinoso, F. The Role of Carbon Materials in Heterogeneous Catalysis. *Carbon* **1998**, *36*, 159–175.
34. Graetz, J. New Approaches to Hydrogen Storage. *Chem. Soc. Rev.* **2009**, *38*, 73–82.
35. Correa, A.; Credendino, R.; Pater, J. T. M.; Morini, G.; Cavallo, L. Theoretical Investigation of Active Sites at the Corners of $MgCl_2$ Crystallites in Supported Ziegler−Natta Catalysts. *Macromolecules* **2012**, *45*, 3695–3701.
36. Fichtner, M. Properties of Nanoscale Metal Hydrides. *Nanotechnology* **2009**, *20*, 204009.
37. Roduner, E. Size Matters: Why Nanomaterials Are Different. *Chem. Soc. Rev.* **2006**, *35*, 583–592.
38. Bondi, A. Van der Waals Volumes and Radii. *J. Phys. Chem. C* **1964**, *68*, 441–451.
39. Wagner, L. K.; Majzoub, E. H.; Allendorf, M. D.; Grossman, J. C. Tuning Metal Hydride Thermodynamics *via* Size and Composition: Li-H, Mg-H, Al-H, and Mg-Al-H Nanoclusters for Hydrogen Storage. *Phys. Chem. Chem. Phys.* **2012**, *14*, 6611–6616.
40. Lee, J.; Farha, O. K.; Roberts, J.; Scheidt, K. A.; Nguyen, S. T.; Hupp, J. T. Metal−Organic Framework Materials as Catalysts. *Chem. Soc. Rev.* **2009**, *38*, 1450–1459.
41. Massiot, D.; Fayon, F.; Capron, M.; King, I.; Le Calvé, S.; Alonso, B.; Durand, J.-O.; Bujoli, B.; Gan, Z.; Hoatson, G. Modelling One- and Two-Dimensional Solid-State NMR Spectra. *Magn. Reson. Chem.* **2002**, *40*, 70–76.